Supplementary Information for

Afterglow-intensity-ratio-based temperature sensing using a persistent phosphor

Chuan Liao,[a,b] Feng Chen,[c] Hao Wu,[a] Huajun Wu,[a] Liangliang Zhang,[a] Guo-hui Pan,[a]

Feng Liu,[c,*] Xiao-jun Wang,[d,†] and Jiahua Zhang[a,b,‡]

[a] State Key Laboratory of Luminescence and Applications,

Changchun Institute of Optics, Fine Mechanics and Physics, Chinese Academy of Sciences,

3888 Eastern South Lake Road, Changchun, 130033, China.

[b] Center of Materials Science and Optoelectronics Engineering,

University of Chinese Academy of Sciences, Beijing, 100049, China.

[c] Key Laboratory for UV-Emitting Materials and Technology of Ministry of Education,

Northeast Normal University, Changchun, 130024, China.

[d] Department of Physics, Georgia Southern University, Statesboro, GA 30460, USA.

* fengliu@nenu.edu.cn

† xwang@georgiasouthern.edu

‡ zhangjh@ciomp.ac.cn

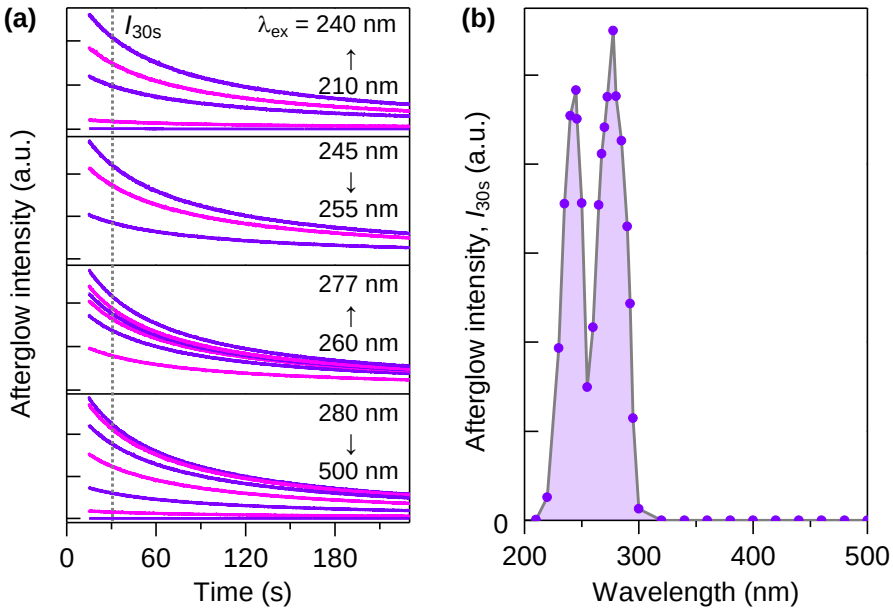

Fig. S1. (a) Afterglow decay curves of $Y_3Al_2Ga_3O_{12}:Pr^{3+}$ monitored at 300 nm ($4f^15d^1 \rightarrow 4f^2$) after irradiated by different wavelengths (210–500 nm) for 5 min at room temperature. The vertical gray line is used to indicate the afterglow intensity at 30 s after the cessation of irradiation (I_{30s}). **(b)** Conventional afterglow excitation spectrum of $Y_3Al_2Ga_3O_{12}:Pr^{3+}$.

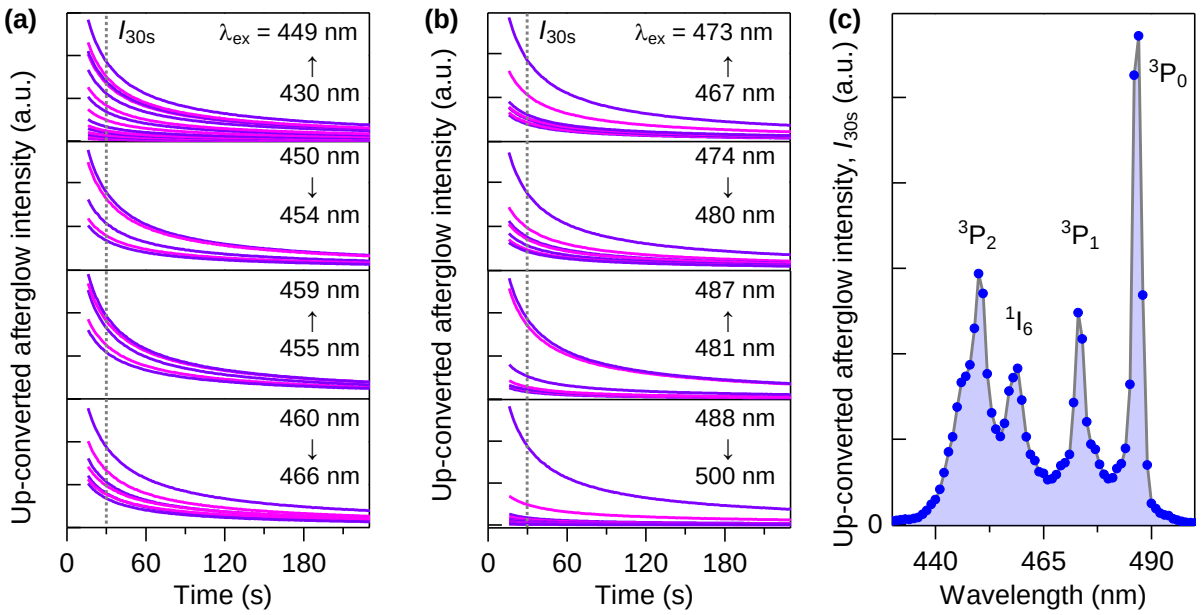

Fig. S2. (a-b) Up-converted afterglow decay curves of $Y_3Al_2Ga_3O_{12}:Pr^{3+}$ phosphor monitored at 300 nm ($4f^15d^1 \rightarrow 4f^2$) after irradiated by different wavelengths (430–500 nm) for 5 min at room temperature. The vertical gray line is used to indicate the up-converted afterglow intensity at 30 s after the cessation of irradiation (I_{30s}). **(c)** Up-converted afterglow excitation spectrum of $Y_3Al_2Ga_3O_{12}:Pr^{3+}$ phosphor.

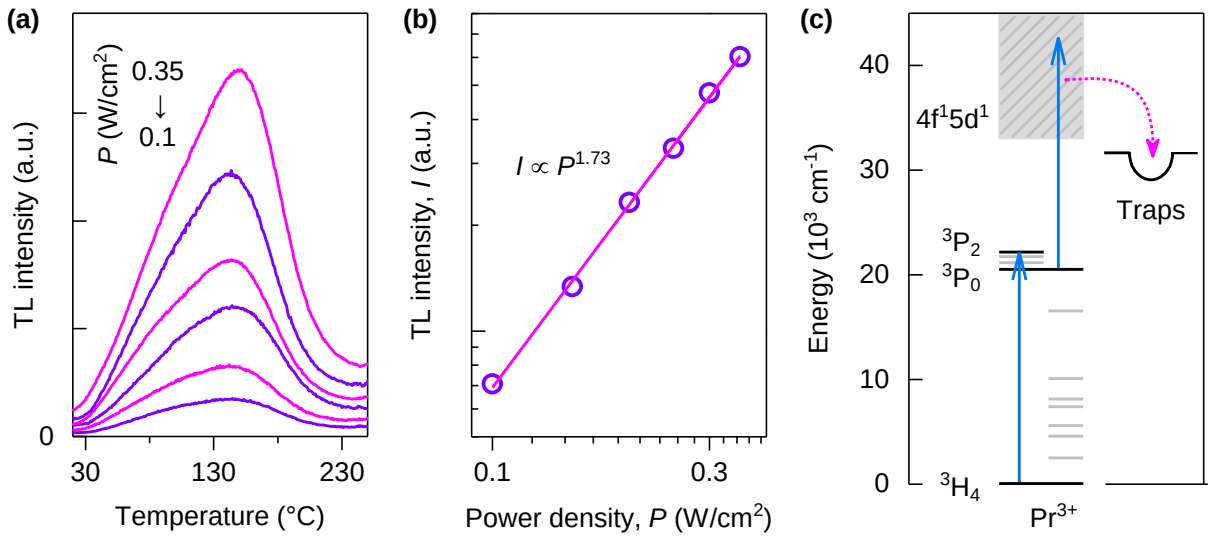

Fig. S3. (a) Thermoluminescence (TL) glow curves of $Y_3Al_2Ga_3O_{12}:Pr^{3+}$ phosphor monitored at 487 nm ($^3P_0 \rightarrow {}^3H_4$) after irradiated by different 455 nm laser power densities. **(b)** The integrated TL intensity (I) was plotted on double-logarithmic scale against the excitation power density (P). The equation of the fitting curve is $I \propto P^{1.73}$. The indicates that blue light can charge the phosphor through a two-photon process. [1,2] **(c)** Schematic diagrams of the two-photon upconversion charging (UCC) process in $Y_3Al_2Ga_3O_{12}:Pr^{3+}$.

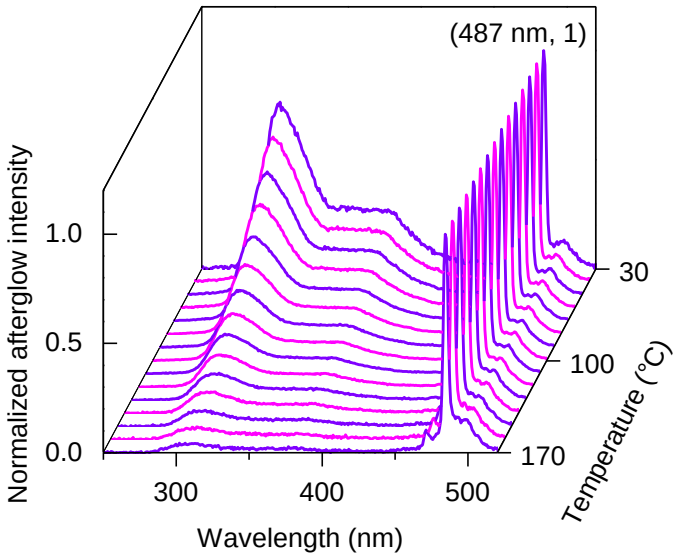

Fig. S4. Afterglow emission spectra of $Y_3Al_2Ga_3O_{12}:Pr^{3+}$ phosphor in air at 5 s after the stoppage of the 254 nm irradiation in the range of 30–170 °C. These spectra are normalized by emission intensity at 487 nm ($^3P_0 \rightarrow {}^3H_4$).

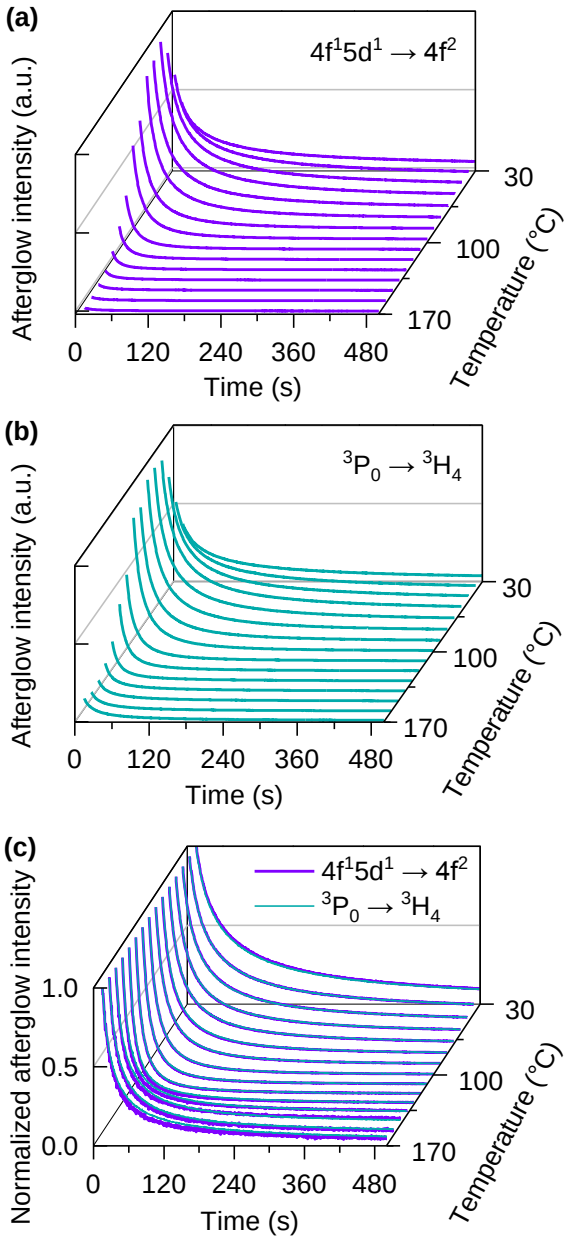

Fig. S5. Afterglow decay curves of $Y_3Al_2Ga_3O_{12}:Pr^{3+}$ phosphor monitored at **(a)** 300 nm ($4f^15d^1 \rightarrow 4f^2$) and **(b)** 487 nm ($^3P_0 \rightarrow {}^3H_4$) after irradiation by 254 nm ultraviolet for 10 min in the range of 30–170 °C. After being irradiated by 254 nm ultraviolet light for 10 min, the traps of the phosphor can be totally filled. **(c)** Normalized afterglow decay curves of the phosphor at different temperatures. The two normalized afterglow decay curves at the same temperature almost completely overlap.

Analysis of afterglow intensity ratio of the $4f^1 5d^1 \rightarrow 4f^2$ to $^3P_0 \rightarrow {}^3H_4$

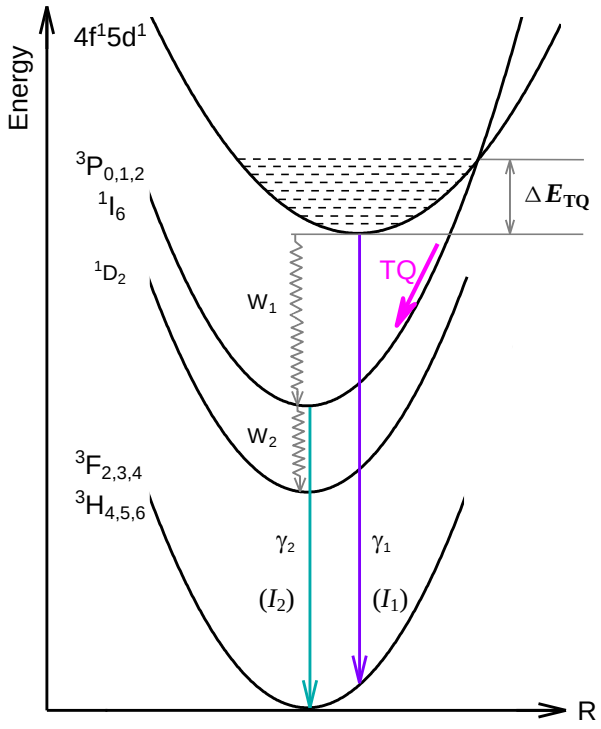

Fig. S6. Schematic diagram of TQ of $4f^1 5d^1$ to $^3P_0$ of Pr^{3+}.

The schematic diagram of thermal quenching (TQ) of $4f^1 5d^1$ to $^3P_0$ of Pr^{3+} is shown in **Fig. S6**. To simplify the analysis, the $^3P_{0,1,2}$ and $^1I_6$ states are only represented by a parabola. The $^3P_0$ state is populated from multi-phonon relaxation (MPR) and TQ relaxation of the $4f^1 5d^1$ state. The pathways for the depopulation of the $^3P_0$ state include MPR and radiative transition. Then we have the steady state rate equations

$$(W_1 + TQ)N_1 = (W_2 + \gamma_2)N_2 \tag{S1}$$

with

$$TQ = A\exp\left[-\frac{\Delta E_{TQ}}{k_B(T+273)}\right] \tag{S2}$$

where W_1 and TQ is the $4f^1 5d^1 \rightarrow {}^3P_0$ MPR and thermal quenching relaxation rates, respectively, W_2 and γ_2 is the $^3P_0 \rightarrow {}^1D_2$ MPR and $^3P_0 \rightarrow {}^3H_4$ radiative transition rates, respectively, N_1 and

N_2 are populations of the $4f^15d^1$ and $^3P_0$, respectively, A is a constant, ΔE_{TQ} (eV) is the compound activation energy of the $^3P_0$, $^3P_1$, $^1I_6$ and $^3P_2$ for thermal quenching, k_B (eV· K^{-1}) is the Boltzmann constant, T (°C) is temperature. [3,4] Since the emission intensity is positively associated to the population of energy levels, the afterglow intensity ratio (AIR) of $4f^15d^1 \rightarrow 4f^2$ (I_1) to $^3P_0 \rightarrow {}^3H_4$ (I_2) can be expressed by the following equation

$$\mathrm{AIR}(T) = \frac{I_1}{I_2} = \frac{\gamma_1 N_1}{\gamma_2 N_2} = \frac{\mathrm{AIR}_0}{1 + \alpha \exp\left[-\frac{\Delta E_{TQ}}{k_B(T+273)}\right]} \quad \text{(S3)}$$

where γ_1 and γ_2 is the $4f^15d^1 \rightarrow {}^3H_{4,5,6}$, ${}^3F_{2,3,4}$ and $^3P_0 \rightarrow {}^3H_4$ radiative transition rate, respectively, $\mathrm{AIR}_0 = \gamma_1(W_2+\gamma_2)/(\gamma_2 W_1)$ is the value of the AIR (T) parameter in the limit $T \rightarrow$ -273 °C, $\alpha = A/W_1$. The TQ process is strongly temperature dependent, while the MPR and radiative transition is less sensitive to temperature compared to TQ. So W_1, γ_1, W_2 and γ_2 can all be considered constants. [5,6]

Note that in addition to the thermally activated crossover quenching pathway, the luminescence of the $4f^15d^1$ state of Pr^{3+} in $Y_3Al_2Ga_3O_{12}$ can also be quenched by thermal ionization and autoionization pathways, but it is still reasonable to use the single barrier quenching model. More details about the $Y_3Al_2Ga_3O_{12}$:Pr^{3+} luminescence quenching is given in ref. [7,8].

Table S1. Fitting parameters of AIR (I_1/I_2) experimental data.

Parameter	Value
AIR_0	17.3293±1.06257
α	66819.92895±27363.3293
ΔE_{TQ} [eV]	0.31095±0.01476
T [°C]	30–170
R^2	0.9994

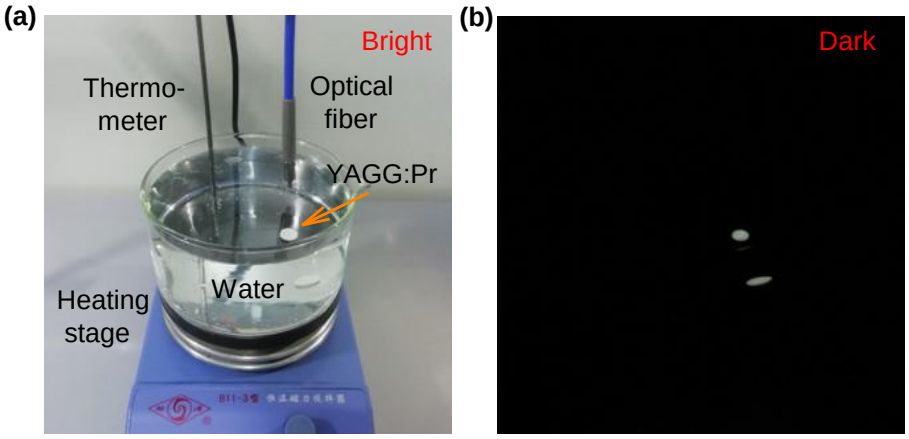

Fig. S7. (a) Experimental device for afterglow intensity ratio (AIR) calibration of $Y_3Al_2Ga_3O_{12}:Pr^{3+}$ (YAGG:Pr) phosphor disk in water. The water depth is 5.5 cm, and the optical fiber probe (perpendicular to the water surface) is 1.5 cm above the water surface. The temperature of water is adjusted by BII-3 type constant temperature heater (BII-3, Sile Shanghai, China) and its own thermometer. After holding each temperature for 5 min, the phosphor disk was charged with a 254 nm ultraviolet mercury lamp for 3 min. **(b)** After charging, afterglow emission spectra of the phosphor disk were recorded with a charge-coupled device (CCD) spectrometer (QEPro, Ocean Optics, China) connected with the optical fiber probe in a dark environment. Optical fiber diameter, 600 μm; spectrometer slit, 100 μm; integration time, 5 s.

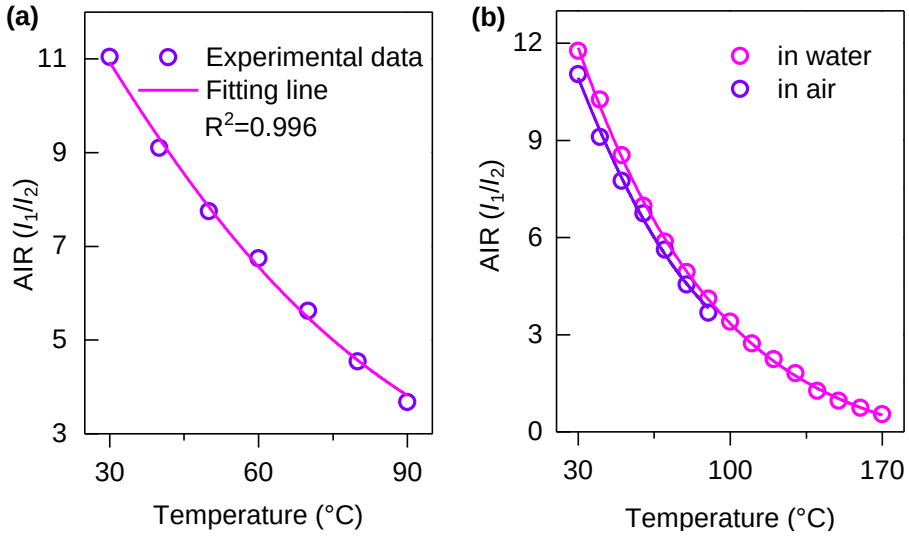

Fig. S8. (a) Afterglow intensity ratio (AIR) of the $4f^{1}5d^{1} \rightarrow 4f^{2}$ (I_1 within 280–450 nm) to $^{3}P_{0} \rightarrow {}^{3}H_{4}$ (I_2 within 480–490 nm) as function of temperature in water (depth: 5.5 cm), and the corresponding fitting line. **(b)** Comparison of AIR (I_1/I_2) measured in water and air. Due to the different absorption coefficients of water to different wavelengths, there are some differences in the AIR (I_1/I_2) values calibrated in water and in air.

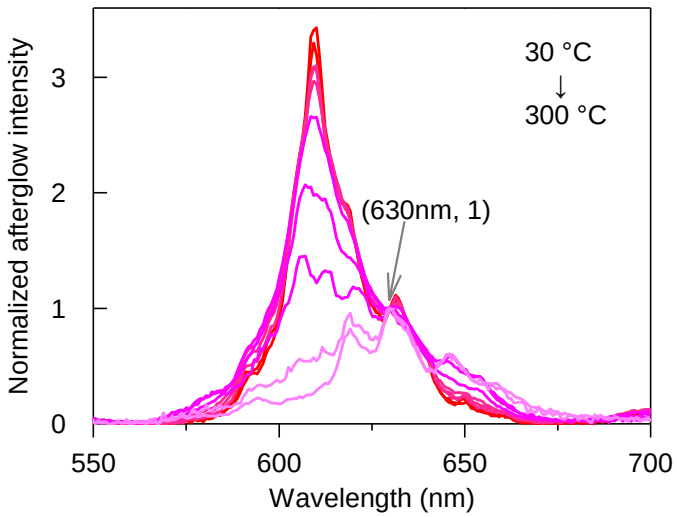

Fig. S9. Normalized afterglow emission spectra of Lu_2SiO_5:0.05%Pr^{3+} after the stoppage of the 254 nm irradiation in the range of 30–300 °C with a step size of 30 °C. This material uses the afterglow intensity ratio for temperature sensing.

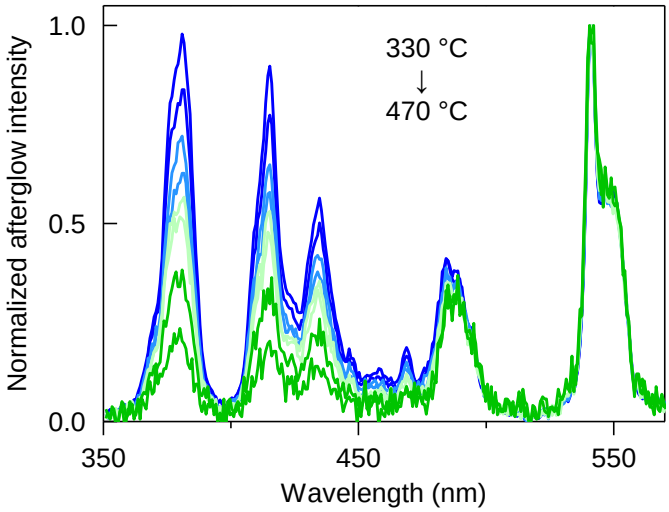

Fig. S10. Normalized afterglow emission spectra of $Y_3Al_5O_{12}$:0.2%Tb^{3+},0.1%Eu^{3+} after the stoppage of the 254 nm irradiation in the range of 330–470 °C with a step size of 20 °C. This material uses the afterglow intensity ratio for temperature sensing.

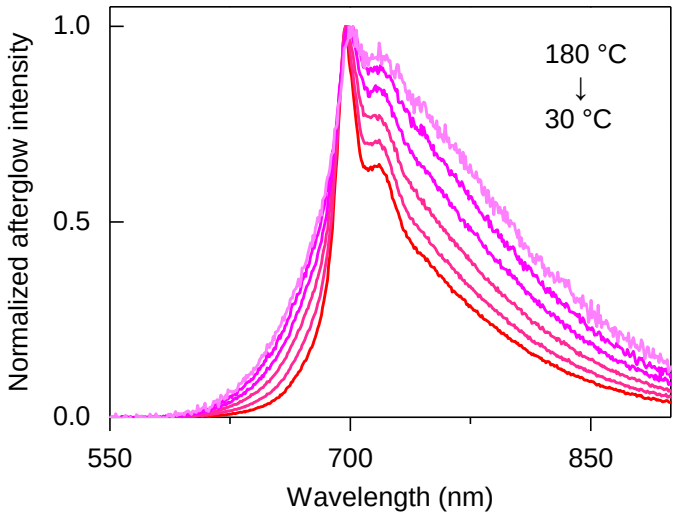

Fig. S11. Normalized afterglow emission spectra of $ZnGa_2O_4$:1%Cr^{3+} after the stoppage of the 254 nm irradiation in the range of 30–180 °C with a step size of 30 °C. This material uses the afterglow emission spectral bandwidth or afterglow intensity ratio for temperature sensing.

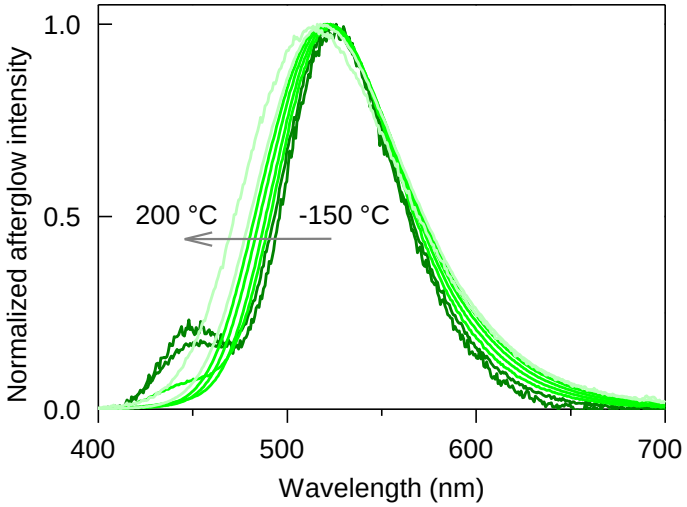

Fig. S12. Normalized afterglow emission spectra of $SrAl_2O_4$:1%Eu^{2+},2%Dy^{3+} after the stoppage of the 450 nm irradiation in the range of -150–200 °C with a step size of 50 °C. This material uses the afterglow emission spectral peak position or afterglow intensity ratio for temperature sensing.

References

[1] X. Zhao, C. Li, F. Liu and X. Wang, *J. Rare Earth.*, 2021, **39**, 1492.

[2] F. Liu, Y. Liang and Z. Pan, *Phys. Rev. Lett.*, 2014, **113**, 177401.

[3] K. Huang, *Prog. In Phys.*, 1981, **1**, 31.

[4] K. R. German, A. Kiel and H. Guggenheim, *Phys. Rev. B*, 1975, **11**, 2436.

[5] B. Ca Nny and D. Curie, *Non-Radiative Relaxation of Solids: Different Pathways to the Ground State*, Advances in Nonradiative Processes in Solids, 1991.

[6] J. Zhang, Z. Hao, J. Li, X. Zhang, Y. Luo and G. Pan, *Light: Sci. Appl.*, 2015, **4**, e239.

[7] J. Ueda, A. Meijerink, P. Dorenbos, A. J. J. Bos and S. Tanabe, *Phys. Rev. B*, 2017, **95**, 014303.

[8] S. Yan, F. Liu, J. Zhang, X. Wang and Y. Liu, *Phys. Rev. Appl.*, 2020, **13**, 044051.